

A nonconformal domain decomposition scheme for the analysis of multiscale structures

Original

A nonconformal domain decomposition scheme for the analysis of multiscale structures / ECHEVERRI BAUTISTA, MARIO ALBERTO; Vipiana, Francesca; Francavilla, MATTEO ALESSANDRO; TOBON VASQUEZ, JORGE ALBERTO; Vecchi, Giuseppe. - In: IEEE TRANSACTIONS ON ANTENNAS AND PROPAGATION. - ISSN 0018-926X. - STAMPA. - 63:8(2015), pp. 3548-3560. [10.1109/TAP.2015.2430873]

Availability:

This version is available at: 11583/2626386 since: 2021-03-30T22:55:17Z

Publisher:

Institute of Electrical and Electronics Engineers Inc.

Published

DOI:10.1109/TAP.2015.2430873

Terms of use:

This article is made available under terms and conditions as specified in the corresponding bibliographic description in the repository

Publisher copyright

IEEE postprint/Author's Accepted Manuscript

©2015 IEEE. Personal use of this material is permitted. Permission from IEEE must be obtained for all other uses, in any current or future media, including reprinting/republishing this material for advertising or promotional purposes, creating new collecting works, for resale or lists, or reuse of any copyrighted component of this work in other works.

(Article begins on next page)

A Non-conformal Domain Decomposition Scheme for the Analysis of Multi-scale Structures

M. A. Echeverri Bautista, *Student member, IEEE*, F. Vipiana, *Senior Member, IEEE*,
M. A. Francavilla, *Member, IEEE*, J. A. Tobon Vasquez, G. Vecchi, *Fellow, IEEE*

Abstract—We present a Domain Decomposition (DD) framework for the analysis of impenetrable structures; it allows for the EFIE and CFIE, and for open, closed, and open-closed structures. The DD results in an effective preconditioner for large and complex problems exploiting iterative solution and fast factorizations. The domain decomposition employs specialized transmission conditions among the domains, and the use of discontinuous Galerkin (DG) allows conformal as well as non-conformal discretizations of domain boundaries; the nonconformal nature of the decomposition gives considerable flexibility in the meshing. The strategy is highly parallelizable, as all the operations involving the sub-domains can be performed in parallel. The proposed scheme is implementation independent and can be easily merged with existing electromagnetic codes.

Index Terms—Integral equations, Domain-Decomposition, Tear-and-Interconnect, Preconditioning, Fast solvers, Moment methods

I. INTRODUCTION

Due to its high accuracy the Electric Field Integral Equation (EFIE) [1] is one of the most used formulation for the analysis of complex structures, and it allows open surfaces; when closed portions of the body are at, or above the resonant length, it needs to be used together with the Magnetic Field Integral Equation (MFIE) into the Combined Field Integral Equation (CFIE) that is resonance-free (e.g. [2]).

The use of fast solvers is mandatory to solve any real-life large problem (e.g. [3]–[7]). All fast factorization store near field interactions, which can then be used by preconditioner without affecting memory scaling of the overall method.

The incomplete LU (ILU) [8] approach is the most employed general-purpose preconditioner in electromagnetics [9], [10]; it is well known though that multiscale problems are not effectively addressed by ILU (e.g. [11]), and the preconditioning of large multi-scale problems has received significant attentions in the past years. For example, multiresolution-based approaches [11]–[14] have been successful in addressing the multi-scale issue for problems up to a few tens of wavelengths.

For electrically large problems, the only “physics based” approaches are apparently those based on the domain decomposition (DD) paradigm at-large [15]–[21]. When adopted in an iterative scheme, the general idea is to extend the block-diagonal preconditioning for a collection of separated scatterers to a large body. In this endeavor, Tear-and-Interconnect DD methods based on transmission conditions are relatively recent in Integral-Equation approaches; they are directly oriented to iterative, fast-factorization based solution, and – as their earlier FEM counterpart – they aim at reducing the iteration

count for electrically large problems [22], [23]. They aimed at curing both the (weak) iteration count growth due to increasing electrical size, and (strong) slowdown due to the presence of multiple scales. Convergence properties in DD depend on the transmission conditions between sub-domains [24]; in [22] these are implemented by adding an artificial perfect electric conductor (PEC) surface to close each of the subdomains upon tearing; surface current cancellation within each pair of artificial inter-domain surfaces is then enforced in the solution scheme. A recent work [25] proposes an overlapping DD method in which the transmission conditions among the overlapped sub-domains are enforced in each inner solver by using the global near field matrix; a suitably reduced version of the whole near field matrix is used in the inner solvers for each sub-problem.

The DD approach can also significantly reduce the meshing burden if independent meshing of the different sub-domains is allowed without requiring adjacent meshes to be conforming; achieving this important result without compromising accuracy and conditioning properties is the task of so-called non-conformal DD methods [22], [23]. Allowance for non-conformal meshing plays a key role in applications such as design and optimization analyzes; e.g., in antenna siting when attaching an independently meshed antenna to a large platform (e.g. airframe) without having to re-mesh the entire structure, and further allowing reduced-order modeling schemes that are crucial to optimization.

In this paper we propose an innovative domain decomposition scheme that does not require artificial closing surfaces between adjacent (torn) domains; as such, it is applicable to open structures as well as to closed and closed-open structures, and suitable for the EFIE alone as well as for the CFIE. As in all approaches of this class, the scheme effectively works as a preconditioner for large and multi-scale problems.

The proposed scheme is non-conformal in nature, allowing the above-mentioned meshing flexibility. Ability to allow for non-conformal meshes in neighboring domains is obtained via a Discontinuous-Galerkin scheme, and we propose a new way of accelerating the solution of the inner sub-problems by using a modified version of [the dual threshold Incomplete LU factorization ILUTP](#) [10] in order to cope with perturbations introduced in the near field matrix by the presence of discontinuous Galerkin terms.

Finally, while intrinsically based on Discontinuous-Galerkin (for both non-conformal and conformal cases), we propose to extend the separated-domain solutions past the tearing lines; this guarantees effective convergence of the iteration loop.

This is especially straightforward thanks to our avoidance of artificial closing surfaces over adjacent domains. The proposed DD preconditioning strategy is structured as a general framework, and therefore easily applicable to any existing fast solver implementation.

Our work presents conceptual similarities to the approach presented in [25], as well as to the seminal work in [26] (for 2D problems); the work reported in [27] shares some of our goals. Differences and innovations with respect to these works and other literature are significant, as detailed next.

In this work the transmission conditions are enforced along the tearing contours between sub-domains; the work in [22] requires an artificial surface, over which currents and fields subsequently are cancelled out performing integrations that use the so called cement technique [28]. The first, obvious advantage of our approach is the ability to deal with open surfaces, thereby extending its applicability. Another very important advantage is the algorithmic flexibility derived from enforcing transmission on the tearing contours, without adding artificial surfaces: the algorithm can be easily embedded into any existing MoM code and is independent of specific choices for the fast factorizations, the iterative Krylov subspace iterative solvers, preconditioners for each domain, etc.

At a difference with [27], we employ domain enlargement for convergence; we enforce transmission conditions via discontinuous Galerkin and present a new way of accelerating the solution of the inner sub-problems by using a modified version of the ILUTP [10] in order to cope with perturbations introduced to the near field matrix by the presence of discontinuous Galerkin terms.

The main point of departure of our approach from [25] and [26] is in the ability to work with both conformal and non-conformal meshes; we enforce the transmission conditions on the tearing contour, while in [25] the transmission conditions come from the use of a truncated version of the global near field matrix for each sub-domain plus a buffer zone (with a constant number of cells) between the sub-domains. While of subtler nature, the difference in algorithmic structure is also an important difference between our work and that in [25]. In [25] the far field blocks of the sub-domains are the same as used in the outer iterations, while in our scheme each extended sub-domain matrix is built independently (with a much lower accuracy, and cost, with respect to the outer matrix); this allows the use of different fast factorizations in different domains, that can thus be tailored to domain properties (e.g. one can use FFT-based techniques for nearly-planar sub-domains, while using [Multi-Level Matrix Decomposition](#) [Algoritim MLMDA](#) [5] or the [Adaptive Cross Approximation ACA](#) [6] for the whole problem). Also, in [25] the multi-scale problem is reduced by generating smaller sub-domains; the associated increase of the number of sub-domains potentially increases the necessary communication among nodes in a parallel implementation. Our framework deals with the multi-scale issue by preconditioning each sub-domain independently with a preconditioner tailored on multi-scale characteristics of each sub-domain; therefore, our decomposition depends only on the users needs. Finally, a minor advantage with respect to [25] arises in the size of the buffer region; in [25] the buffer

zone (overlap zone) is formed by a constant number of cells that varies between 8 to 12 cells (0.8 to 1.2λ for a standard $\lambda/10$ discretization); with our scheme we need only a $\lambda/4$ (0.25λ) near field extension.

Summarizing, the inner-outer scheme in our approach aims to solve multi-scale realistic structures where each sub-problem, though possibly electrically small, can be complex and ill conditioned; furthermore, the algorithmic structure of our scheme ensures that each sub-problem be solvable by means of any fast solver and preconditioner independently from others. Therefore, our framework is highly adaptable as it allows the use of different preconditioning strategies within each sub-domain, giving great versatility in complex geometries analysis.

The paper is organized as follows: section II presents some background on integral equations formulations. In section III the new domain decomposition framework is explained. Numerical tests are presented in section IV in order to show the advantages of the developed method. Finally in section V some conclusions and future work perspectives are drawn.

II. BACKGROUND

We consider a PEC body on which the unknown current density \mathbf{J} is approximated as a linear combination of basis functions

$$\mathbf{J}(\mathbf{r}) \simeq \sum_{n=1}^N I_n \mathbf{f}_n(\mathbf{r}) \quad (1)$$

where I_n corresponds to the current expansion coefficients and $\mathbf{f}_n(\mathbf{r})$ to the Rao-Wilton-Glisson (RWG) basis functions [29]; applying the Method of Moments (MoM) and Galerkin testing to the EFIE, the problem is transformed into the linear system:

$$[Z_{\text{EFIE}}][I] = [Z_{\text{EFIE}}^A + Z_{\text{EFIE}}^\phi][I] = [V_{\text{EFIE}}] \quad (2)$$

where

$$Z_{mn}^A = \frac{j\omega\mu_0}{4\pi} \iint_{S_m} dS \mathbf{f}_m(\mathbf{r}) \cdot \iint_{S_n} dS' G(\mathbf{r}, \mathbf{r}') \mathbf{f}_n(\mathbf{r}') \quad (3)$$

$$Z_{mn}^\phi = \frac{1}{j4\pi\omega\epsilon_0} \iint_{S_m} dS \nabla_s \cdot \mathbf{f}_m(\mathbf{r}) \iint_{S_n} dS' G(\mathbf{r}, \mathbf{r}') \nabla_{s'} \cdot \mathbf{f}_n(\mathbf{r}') \quad (4)$$

$$V_m = \iint_{S_m} dS \mathbf{f}_m(\mathbf{r}) \cdot \mathbf{E}_i(\mathbf{r}) \quad (5)$$

with $G(\mathbf{r}, \mathbf{r}') = e^{-jk_0|\mathbf{r}-\mathbf{r}'|}/|\mathbf{r}-\mathbf{r}'|$, $k_0 = \omega\sqrt{\epsilon_0\mu_0}$, S_m and S_n correspond to the supports of the functions \mathbf{f}_m and \mathbf{f}_n respectively, and \mathbf{E}_i to the incident electric field. In (2) we have explicitly denoted the contributions of the scalar (ϕ) and vector (A) potentials. The same discretization strategy is applied to the MFIE, yielding:

$$Z_{mn}^{\text{MFIE}} = \frac{1}{2} \iint_{S_m} dS \mathbf{f}_m(\mathbf{r}) \cdot \mathbf{f}_n(\mathbf{r}) + \frac{1}{4\pi} \iint_{S_m} dS \mathbf{f}_m(\mathbf{r}) \times \hat{n} \cdot \iint_{S_n} dS' \mathbf{f}_n(\mathbf{r}') \times \nabla G(\mathbf{r}, \mathbf{r}') \quad (6)$$

$$V_{m\text{MFIE}} = \iint_{S_m} dS \mathbf{f}_m(\mathbf{r}) \cdot \hat{\mathbf{n}} \times \mathbf{H}_i(\mathbf{r}) \quad (7)$$

where $\hat{\mathbf{n}}$ is the outward unit normal to the surface., and \mathbf{H}_i is the incident magnetic field. The Combined Field Integral Equation (CFIE) is then expressed as a linear combination of EFIE and MFIE as follows:

$$\begin{aligned} (\alpha[Z_{\text{EFIE}}] + (1 - \alpha)[Z_{\text{MFIE}}])[I] &= \\ (\alpha[V_{\text{EFIE}}] + (1 - \alpha)[V_{\text{MFIE}}]) \end{aligned} \quad (8)$$

where $0 < \alpha < 1$ is the weight controlling the contribution of the EFIE and MFIE operators.

III. DOMAIN DECOMPOSITION ALGORITHM

A. Strategy

The general tear-and-interconnect strategy can be seen as the extension of the block-diagonal preconditioning for a collection of separated scatterers; therefore, the overall geometry is torn into a collection of non-overlapping domains (figure 1). The overall matrix equation in (2) is solved iteratively using a (standard) Krylov subspace iterative solver (e.g. GMRES [30]); preconditioning is obtained via individual sub-domains solutions. Formally, this is done via the inverses of the sub-systems for the standalone terminated domains. In order to achieve this preconditioning, it is essential to terminate the domains enforcing the so-called transmission conditions, a crucial ingredient of tear-and-interconnect approaches. Because one usually does not want to compute and store the (fully populated) inverses of the problem for each domain, this operation is done via a separate (and independent) iterative solver (possibly different on each domain). This induces an “outer” iteration loop over the entire structure - which is the usual iterative solver that one would use, and “inner” iteration loops over the individual domains.

An important remark has to be made about the tearing of closed portion when using the CFIE formulation: although the subdomains resulting from tearing are individually open, they belong to a closed body; therefore the formulation used in the subdomains is the same CFIE as for the their closed union.

Finally, one observes that the solutions on the individual domains (inner solvers and inner loops) are all independent, and thus inherently parallel.

The rest of this section is devoted to describe the key ingredients of the proposed DD scheme. Because of its important role in allowing conformal, non-conformal meshes, we begin with a brief description of the discontinuous Galerkin formulation, as specifically applied in our approach; section III-C, explains the proposed method for the improvement of the transmission conditions. Section III-D describes the setup phase to build all the necessary blocks that act as inputs for the Krylov subspace solver. Section III-E illustrates the solution phase, which takes all the pieces computed in the setup phase and use them to solve the linear system (2). Finally the approach proposed as a preconditioner for the inner problems is explained in section III-F.

B. Discontinuous Galerkin

The general framework to deal with structures with non-conformity of meshes is called the Discontinuous Galerkin approach (see [31] for its application to Integral Equation formulations). A generic PEC structure is decomposed in two connected structures (sub-domains or sub-problems) as shown in figure 1 where S refers to the PEC surface being discretized,

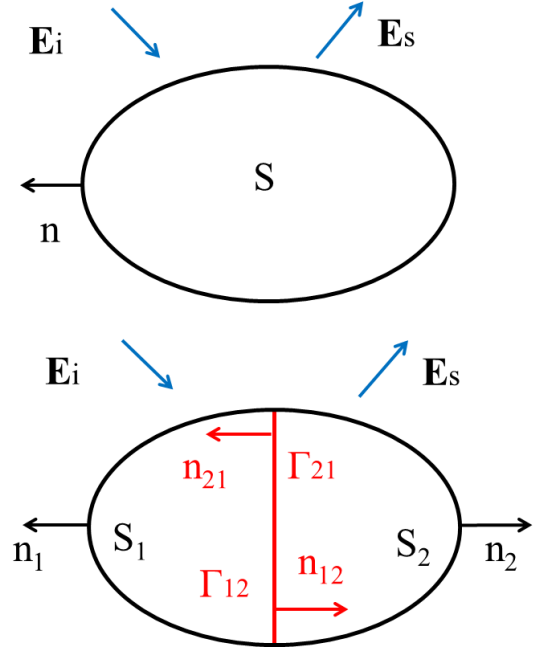


Fig. 1. Geometry decomposition for discontinuous Galerkin approach

E_i and E_s are the incident and scattered fields respectively and $\hat{\mathbf{n}}$ is the unit normal vector to the S surface. In the decomposed problem, the previous attributes are discriminated by the number assigned to each subdomain. Two new attributes appear: Γ_{ij} , the common interface contours between subdomains i and j , and $\hat{\mathbf{n}}_{ij}$ for the unit normal vector to Γ_{ij} pointing outwards domain i .

We do not define RWGs across the contour Γ_{ij} ; instead we define linear basis functions on single mesh cells independently on the two sides of the contour. These basis functions, depicted in figure 2 and referred to as half-RWG (h-RWG in the following), are not div-conforming by construction. As a consequence, charge may accumulate along the artificial cut identified by Γ_{ij} ; the so called interior penalty concept [31] is used to penalize the potential produced by the charges accumulated along the artificial cut. The interior penalty terms are then added to the usual reaction integrals of the EFIE operator. It is remarked that equation 4 is obtained upon applying a vector calculus identity as done in [29] to move the gradient operator from the scalar potential to the testing function. However, for non div-conforming functions, additional contour contributions are necessary (not shown in equation 4 which assumes div-

conforming functions):

$$Z_{mn\text{EFIE}}^{IP} = \frac{1}{j4\pi\omega\epsilon_0} \int_{\Gamma_m} d\Gamma \hat{n}_m \cdot \mathbf{f}_m(\mathbf{r}) \iint_{S_n} dS' G(\mathbf{r}, \mathbf{r}') \nabla_s \cdot \mathbf{f}_n(\mathbf{r}') - \frac{1}{j4\pi\omega\epsilon_0} \iint_{S_m} dS \nabla_s \cdot \mathbf{f}_m(\mathbf{r}) \int_{\Gamma_n} d\Gamma' G(\mathbf{r}, \mathbf{r}') \hat{n}_n \cdot \mathbf{f}_n(\mathbf{r}') \quad (9)$$

where Γ_m is the “free” edge associated to the h-RWG; \hat{n}_m refers to the normal to the m -th edge Γ_m ; A_m is the area of the triangle where the m -th function is defined. In the above, the contour integrals relating potential produced by the normal components and tested onto the normal components have been dropped for consistency with the DG formulation [31]. The stabilization term in [31] was intended for the case dealt with there, i.e. when the DG is used on significant *surface* portions of the structure; it was shown there that it improves the effectiveness of a NF-based preconditioner when the mesh density is increased. At a difference with [31], our use of DG is limited to the cut *contours* only, resulting in a significantly smaller perturbation of the overall linear system; hence, we did not find it necessary to add such a term in our case.

The elements $Z_{mn\text{EFIE}}^{IP}$ are added to the usual Z_{EFIE} terms when computing interactions relating h-RWG. The inclusion of the DG terms (wherever an interaction with a h-RWG is defined) modifies the diagonal dominance of the matrix, creating undesired effects on the conditioning of the matrix [27]. Different approaches to deal with the ill-conditioning arising from the use of DG have been proposed [31], [32]; in this work a different strategy is proposed and explained in section III-F.

C. Tear-line and interconnect

As explained in Sec. III-A the linear system in (2) is left-preconditioned via the solutions of individual domains; this is algebraically expressed as:

$$[M]^{-1}[Z][I] = [M]^{-1}[V] \quad (10)$$

where the matrix $[M]^{-1}$ is the preconditioner; the block diagonal (BD) preconditioner is a suitable option for parallel preconditioning. In a two domains case, $[M]$ has a block structure as the following:

$$[M] = \begin{bmatrix} [M_1] & 0 \\ 0 & [M_2] \end{bmatrix} \quad (11)$$

where the $[M_i]$ block refers to the MoM matrix of domain i ; this MoM matrix is built with a much lower precision (i.e., the fast solver tolerance) than the overall system matrix $[Z]$. This is done to minimize the cost for generating and storing the preconditioner $[M]$, as well as its application (i.e., the cost of the inner loop). The block diagonal preconditioner in (11) although inherently parallelizable, neglects the continuity of the solutions along the contours separating the domains. Effective transmission conditions between connected sub-problems are the corner stone of any DD scheme to improve the convergence of a Krylov subspace iterative solver [22], [24].

Discontinuous Galerkin (DG) is used to establish continuity along the contours dividing the structure; it is in fact the key to reach the conformal and non-conformal capabilities of the scheme. The continuity is enforced by using h-RWG, where the interior penalty concept [31] is used to take into account and penalize the potentials produced by the charges accumulated in the contour. Figure 2 explains the definition of a generic h-RWG, where \mathbf{f}_m stands for the vector function

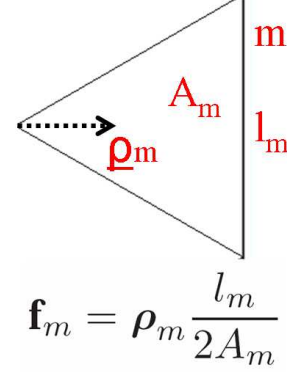


Fig. 2. Definition of a half-RWG (h-RWG).

defining the basis that expands the current in the triangle; the associated edge m is the one where charge accumulates (as opposed to the RWG, which is pair-wise defined, and has an implicit charge cancellation). h-RWGs are employed to expand the current along the contours connecting different domains; figure 3 exemplifies the location of a set of h-RWGs (on the triangles), providing continuity at the interface X between domains A and B .

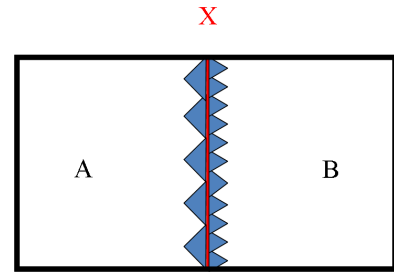


Fig. 3. h-RWGs (on the triangles) are placed along the interface contour X connecting domains A and B , to provide continuity of the solution.

The transmission conditions given by the DG in the cutting contours are not so appealing, as the iterative solver will have to deal with the cancellation of the electric potentials produced by the charges accumulated along the contours; the key to improve the outer convergence is to pass this burden from the outer domain to the inner sub-domains. As the charges are mapped to potentials by means of a convolution with the Green's function of the problem, it is recognized that the near field of the sources (charges) contains enough information to properly account for the cancellation of the potential (in a weak sense). Using this rationale the transmission conditions are established in this work enlarging the sub-domains, by including the “near field” of the adjacent (connected in the original problem) sub-domains, where near field is intended as

usual in fast solvers jargon (e.g. $\lambda/4$). In figure 4 two domains are used, and the transmission conditions are to be enforced. In figure 4 “Dom 1” and “Dom 2” are connected domains

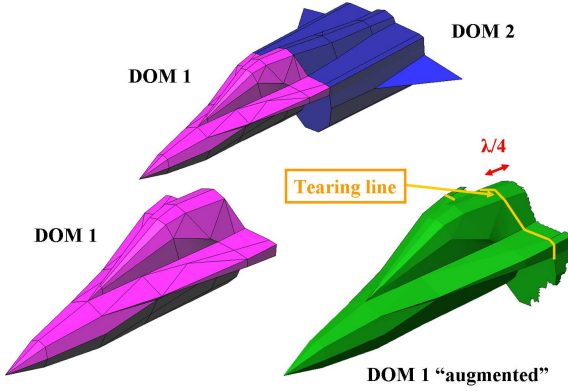


Fig. 4. “Dom 1” is “augmented” by including an overlap region belonging to an adjacent domain (“Dom 2”).

interacting, and “Dom 1 augmented” is the enlarged domain solved in the inner loop for preconditioning “Dom 1”. It is remarked that the tear lines (contours) are included within the enlarged domains.

D. Setup Phase

First, all domains are “augmented” (as explained in section III-C); next, the MoM matrices $[M'_i]$ of the augmented domains are built (using any fast solver available), for $i = 1, \dots, N_D$ where N_D is the number of domains. The matrices $[M'_i]$ are “thin” in the sense that they are built with a lower precision than the matrix $[Z]$. The setup phase is summarized in figure 5. The MoM matrices ($[Z]$ and $[M'_i]$) are built in

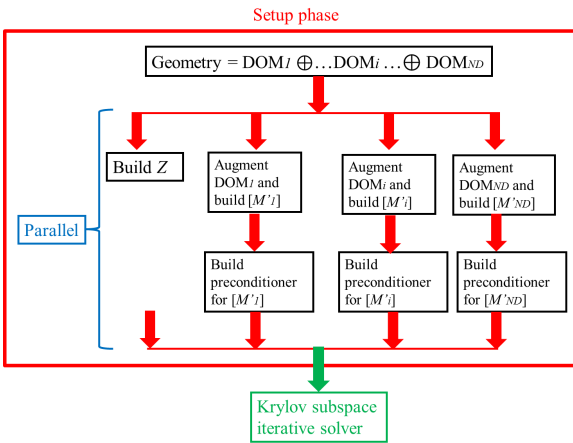


Fig. 5. Setup phase of the proposed scheme: first each domain is “augmented”, then the corresponding system matrices and preconditioners for each domain are generated and stored.

parallel; after each $[M'_i]$ is assembled, the preconditioner to accelerate the convergence of the inner solvers are created (section III-F). Here it is noted that any strategy can be used to parallelize the construction of $[Z]$ (which carries the higher computational burden).

E. Solution Phase

After all matrices $[M'_i]$ and $[Z]$ are built, we resort to a Krylov subspace iterative solver, in our case GMRES [30] for the outer iterative solver. The inner solver is preconditioned using an ILUTP applied to the “augmented” domains as described in section III-F; in fact, as the scheme is general, ILUTP can be replaced by a different preconditioner for the inner problems (possibly different and tailored to each domain). It is remarked here that both construction and application of the preconditioner (e.g. matrices $[M'_i]$) is entirely parallel. The solution phase is schematically outlined (and simplified for the sake of clarity) in figure 6, where primed quantities refer to

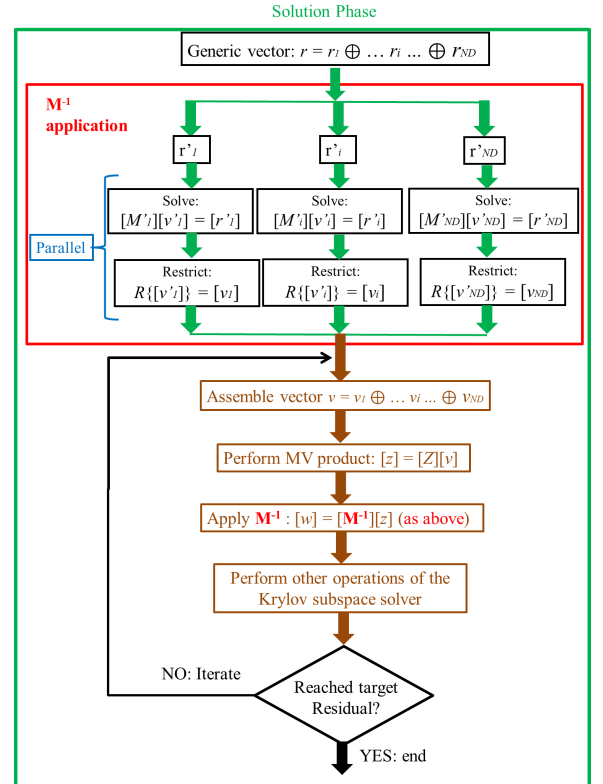


Fig. 6. Flow-chart representation of the solution phase for the proposed scheme.

augmented domains, while non-primed quantities refer to the non conformal, non-overlapping domains. The generic vector r is partitioned into portions relating to individual (augmented) domains: $[r'_i]$ is the portion from r defined on the augmented domain “DOM i ”. The linear systems $[M'_i][v'_i] = [r'_i]$ are iteratively solved (inner solver); the solution $[v'_i]$ is then restricted to the domain “DOM i ” (i.e., the elements belonging to the augmented portion of the domain are dropped) to yield $R_i[v'_i] = v_i$, with $v = v_1 \oplus \dots \oplus v_i \oplus \dots \oplus v_{ND}$ and $v_i \cap v_j = \emptyset, \forall i \neq j$. Once the restrictions of the solution vectors v_i are obtained, the preconditioned outer vector is assembled as the union of the restrictions. The couplings of single domain solutions are then “coupled” by means of a matrix-vector (MV) product.

F. Inner solver preconditioning

For the $[M]^{-1}$ application in figure 6, we first need to solve the inner linear systems $[M'_i][v'_i] = [r'_i]$ and then restrict the solutions $[v'_i]$. For the inner linear systems solutions an iterative solver is used; in order to improve the convergence properties when DG is used (in the inner solvers), we propose here to use the ILUTP [8] preconditioner. The idea is to include the matrix elements involving contour h-RWG (and thus interior penalty terms) into the near field matrix (explained in more detail ahead); figure 7 shows a schematic representation of the MoM matrix and its “fast” representation. where, Z_{RWG} indicates

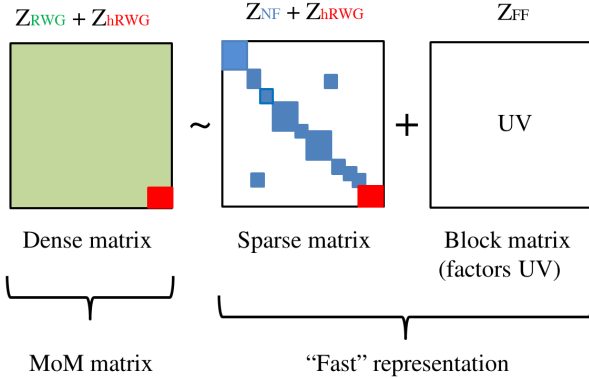


Fig. 7. h-RWG inclusion in the near field matrix; the ILUTP preconditioners for the inner systems are generated with the matrix $Z_{NF} + Z_{hRWG}$, which includes h-RWG contributions, and thus interior penalty terms.

the part of the full MoM matrix that stores the interactions between RWG functions, Z_{hRWG} corresponds to the part of the matrix storing the interactions including the DG terms; Z_{NF} and Z_{FF} are the usual near field and far field matrices of a fast algorithm. In practice what is done is to flag the groups in the near field level (e.g. the smaller groups), to indicate whether or not they contain h-RWG. Then when evaluating if two groups are far or near this flag is observed; if both source and test groups contain h-RWG this block of matrix is included into the NF matrix (even if the two groups could be far from each other). An increase in the memory for the near field matrix is expected; however the number of elements in the contour is typically very small compared to the rest of the problem, and grows as the boundaries (not surfaces) of the domains. As a consequence, this should not pose any limitation to the application of the scheme for practical problems. Then the ILUTP preconditioner is straight-forwardly generated and applied [9], [10]. Here it is observed that a similar strategy has been proposed in [32]; there however the used preconditioner is based on block Jacobi and the only interactions included in the near field are h-RWG vs h-RWG interactions.

IV. NUMERICAL RESULTS

In this section different performed tests are described. The fast solver used is the Adaptive Cross Approximation (ACA), with compression tolerance 10^{-3} (for matrix Z in figure 5) unless otherwise specified; the sub-problems matrices for the DD preconditioner are instead compressed with tolerance

of only 10^{-1} (matrices $[M'_i]$ in figure 5). The inner and outer iterative solver used is the GMRES [30]; the residual required to the outer GMRES is 10^{-6} (residual of the outer solver in decision rhombus in figure 6), while for the inner GMRES the residual is only 10^{-3} (residual for iteratively solving inner systems $[M'_i][v'_i] = [r'_i]$ in figure 6). The outer residual has been chosen for testing the stability of the outer iterations, for most applications 10^{-4} would suffice; the values for inner residual and inner compression tolerance give a good trade-off between inner computational burden and outer convergence. Single-domain results refer to the case where neither decomposition nor discontinuous Galerkin are used; multi-domain refer to the case where the structure has been decomposed and discontinuous Galerkin is used in the contours between connected sub-domains; in both cases ILUTP preconditioner has been used (as described in section III-F when discontinuous Galerkin is used). For open/closed structures the EFIE operator is applied to the open parts, while CFIE (with $\alpha = 0.5$) is applied on the closed ones. Section IV-A is devoted to the assessment of the inner solver acceleration scheme explained in section III-F, while the rest of the numerical results are associated to the proposed DD algorithm. All the simulations are performed with an Intel Xeon ES-2670 (2.6 GHz), 64-bit server with 256 GB of RAM.

A. Inner Subdomain Solver Acceleration

In this part the preconditioning scheme proposed in section III-F for the inner solvers is tested. A plane wave impinges axially on a PEC cylinder (2 m height, 0.5 m radius, figure 8); both the single domain cylinder and the decomposed domain (4 domains using DG at the discontinuities) are simulated using the CFIE formulation. Figure 8 shows both single and 4-domain meshes (conformal mesh). The simulation frequency is 600 MHz; the mesh discretization is kept the same for both cases ($h \approx 0.05$ m); the number of unknowns for single domain is 12906 unknowns (RWG), while the 4-domain case have 12420 (12042 RWG + 378 h-RWG). Table I shows the computational statistics for this simulation; In table I FF refers to far field memory, NF stands for near field; ILU is the memory occupied by the incomplete LU factorization made using the near field matrix. $TOT = FF + NF + ILU$ is the total memory used by the schemes. $Solv. Time$ is the time it takes to achieve the required residual (iterative solver) and $Iter$ refers to the number of iterations performed by each scheme. Both approaches are preconditioned using the ILU preconditioner; in the DG case the inclusion of the h-RWG and neighbors interactions have been included in the near field matrix as described in section III-F. Figure 9 shows the results obtained for both single domain and 4 domains; both current density and bistatic RCS are presented. The results obtained with the strategy proposed in section III-F have excellent agreement with those for the single domain (which obviously has no h-RWG).

B. Convergence behaviour with frequency

In this section the convergence of the proposed scheme is assessed against frequency, leaving the number of sub-domains

TABLE I
INNER PRECONDITIONER PERFORMANCES WHEN USING DG IN CONTOURS, PEC CYLINDER CASE

Case	FF. Mem. (MB)	NF. (MB)	ILU (MB)	TOT. (MB)	Solv. Time (s)	Iter
<i>FULL+ILU</i>	682.35	62.27	118.7	863.32	1.961	13
<i>DG+ILU</i>	620.9	71.29	135.9	828	2.215	14

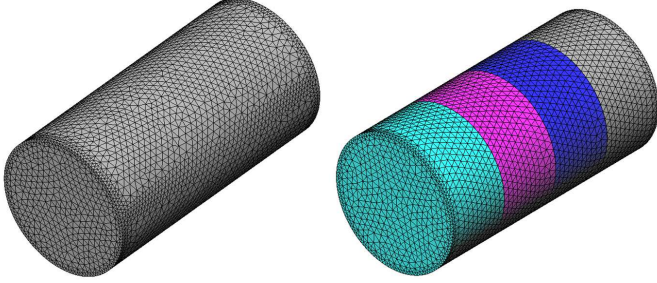


Fig. 8. Full and domain decomposed PEC cylinder

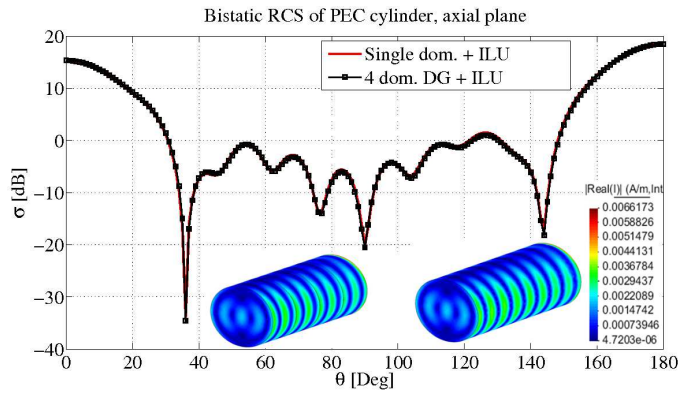


Fig. 9. Full and domain decomposed PEC cylinder, current density and bistatic RCS

unchanged. The number of iterations is accounted for three different frequencies (300, 600 and 1200 MHz) using the CFIE formulation. The test case is a plane wave impinging axially a PEC cylinder divided in 4 domains (conformal mesh); an average discretization of $h \approx 0.025$ m is used. The cylinder is 2 m height and has radius of 0.5 m; The total number of unknowns is 51117. The results of this test are shown in figure 10. where the height of the cylinder has been specified in λ .

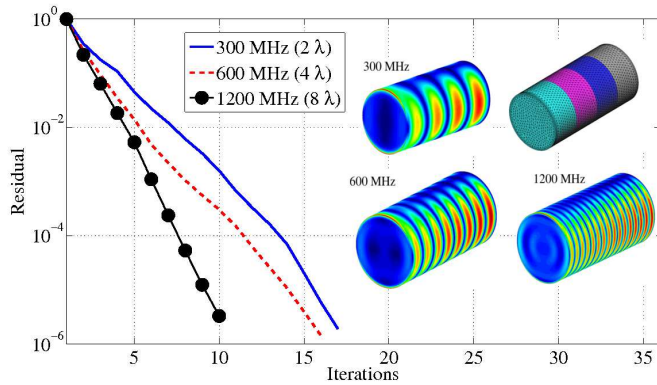


Fig. 10. Scaling of number of iterations

As expected, the computational load is translated from the outer to the inner solvers (for a constant residual). In this case, the number of iterations of the inner solver increases (on average) from 15 to 25 to achieve the specified residual; however, we observe that this is the part that is performed in parallel (solution phase in figure 6).

C. Convergence Behavior with Number of Domains

We now investigate on the effect of the number of sub-domains, keeping the frequency constant. The test structure is a PEC sphere with radius 0.5 m impinged by a 3 GHz plane wave (the sphere is 10λ in extent); the CFIE formulation is used. The comparison is performed between the single domain sphere, and three different decomposition analyzed with our approach. The decomposed geometries are three: 2 sub-domains, 4 sub-domains and 8 sub-domains (figure 11); meshes are conformal. The ILU preconditioner is used to precondition the inner problems but any other preconditioning technique can be used here. The number of unknowns for the single domain sphere is 132 468 RWG, while the two domains decomposition uses 131 328 RWG + 1 248 h-RWG, the four domains decomposition uses 130 704 RWG + 2 496 h-RWG and the eight domains decomposition uses 126 672 RWG + 5 088 h-RWG. In figure 12 the imaginary part of the equivalent

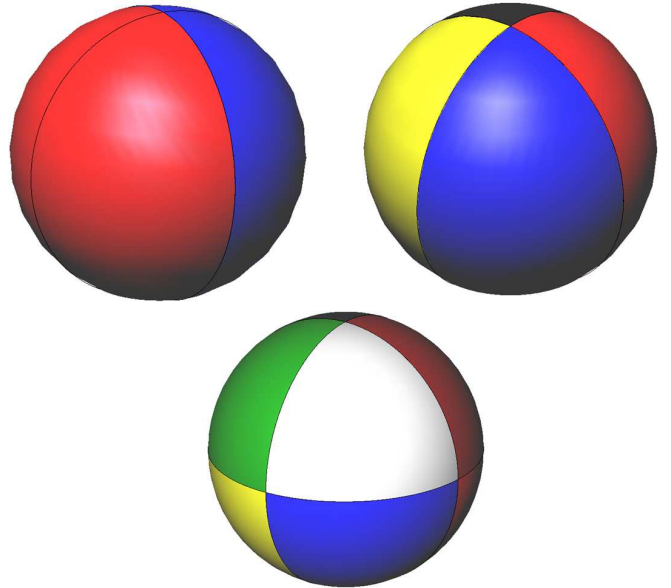


Fig. 11. Geometry decomposition

current densities for all test cases are presented. From figure 12 an excellent agreement between the solutions of the single domain problem and the different geometrical decomposition is noted. The convergences for the different cases are presented in figure 13. The increase in the number of iterations was

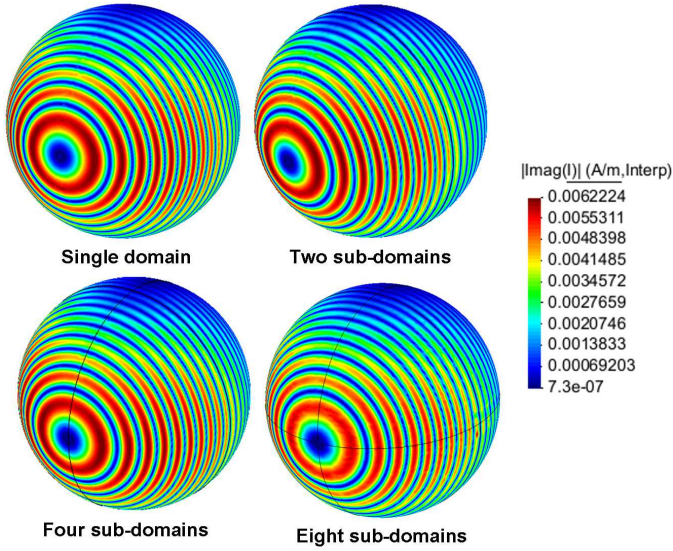


Fig. 12. Imaginary part of the equivalent current density

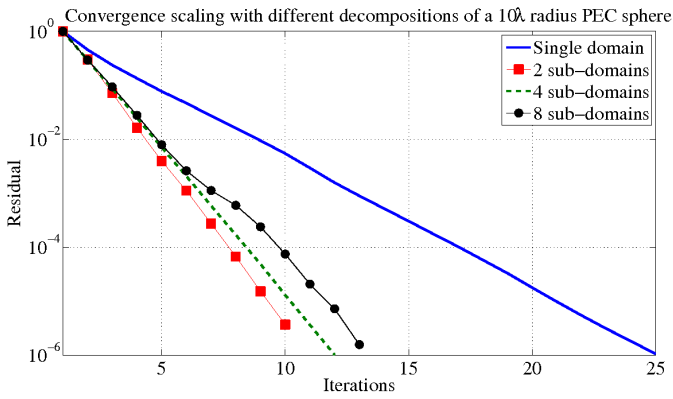


Fig. 13. Iterations count for the different test test cases

to be expected, and has been explained in a detailed way in [33], and briefly summarized here. The eigenvalues related to evanescent modes are the most problematic to be clustered; these evanescent modes decay within a zone depending on the simulation frequency; for a fixed frequency, by increasing the number of domains the domains become smaller, giving rise to reflections of the evanescent modes (as they no longer decay within the domain), and this is what ultimately causes the increase in the iterations count of the outer solver. A trade-off between number of domains and the time for solving the outer problem arises; this trade-off is also affected by the complexity of the structure, as will be seen in the next section.

D. Non-conformal Mesh

In this section the ability to handle non-conformal meshes is demonstrated. A PEC cone (height = 2 m, base radius = 0.8 m, figure 14) is divided in four sections, meshed with different densities (the same test case has been proposed in [31]); here the EFIE formulation alone is used. The simulation frequency is 300 MHz and the mesh densities used are $\lambda/40$, $\lambda/20$, $\lambda/10$ and $\lambda/5$; the relative residual is set to 10^{-5} (outer

GMRES). The reference *single domain* cone is discretized with $\lambda/12$ density (to obtain a similar number of unknowns). The test cases are presented in figure 14 (single and decomposed cases); the bistatic RCS for a vertically polarized plane wave impinging from the tip-to-base direction are shown in figure 15, that validates the correctness of the proposed DD-DG.

Finally the convergence of the compared schemes are presented in figure 16; for this case the required residual for the outer GMRES is 10^{-5} while the inner one is 10^{-2} ; these results show that the convergence acceleration remains also in the non-conformal case with the proposed DD-DG.

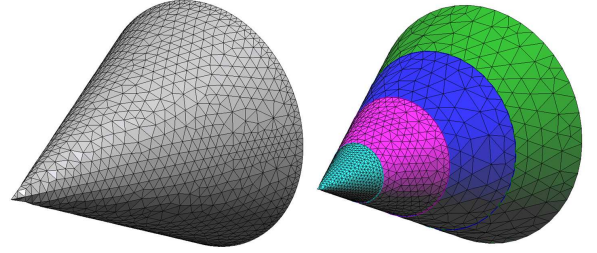


Fig. 14. Non-conformal mesh test case; single and decomposed domains

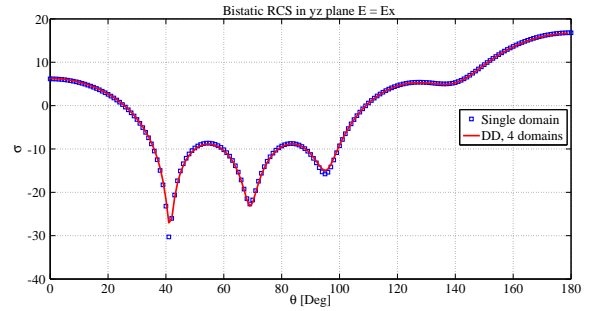


Fig. 15. Non-conformal mesh handling

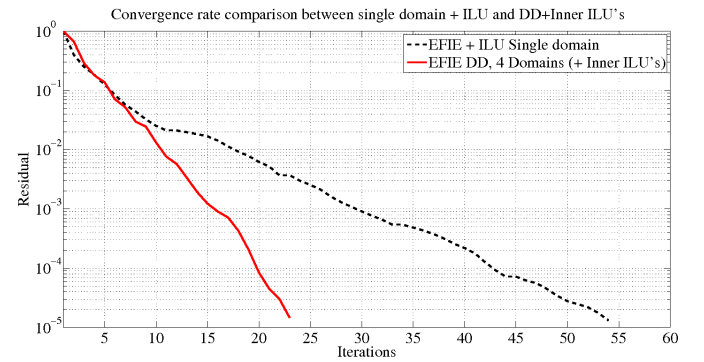


Fig. 16. Non-conformal mesh handling, iterations

E. Complex Multi-scale Test Case

In this section a multi-scale structure is analyzed. The test case is a 600 MHz plane wave impinging a morphed version of the Rafale aircraft (figure 17). The Rafale has been decomposed in thirteen, independently meshed parts (figure 18),

thus resulting in non-conformal meshes, as shown in Fig. 19; two blade antennas are placed on the airplane (one below the cockpit, one in the back of the cockpit), while each rocket has a small fin with the same dimensions as the blade antennas; the antennas (and fins) have been meshed with a discretization size of $\lambda/1000$; the wings and tail-wing have been discretized at $\lambda/10$; the central body is discretized at $\lambda/11$; the cockpit has been discretized at $\lambda/12$, with the exception of the lower part around the blade antenna; the domains surrounding the blade antennas and the rockets have been discretized at $\lambda/17$. Details of some of the non-conformal characteristics of the mesh are shown in figure 19; this test case combines both conformal and non-conformal characteristics in the different interfaces among the sub-domains. The CFIE is used in the closed parts (the entire aircraft is closed) and the EFIE is used in the blade antennas, rocket wings and attachment bays (open structures); the blade antennas and rocket fins are about $\lambda/4$ at the simulation frequency. Discretization size varies as $5 \times 10^{-4} < h/\lambda < 5 \times 10^{-2}$, the length (tail to tip) of the aircraft is 28λ and the number of unknowns is 301 295 (297 310 RWG + 3985 h-RWG). The current density

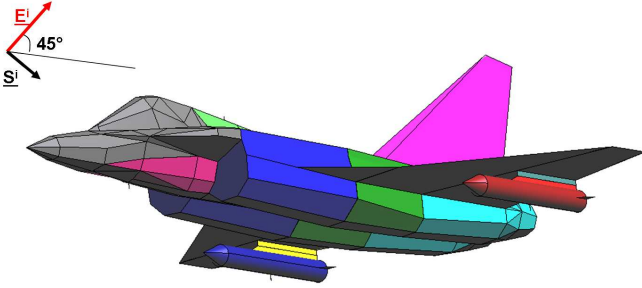


Fig. 17. Plane wave impinging on morphed Rafale

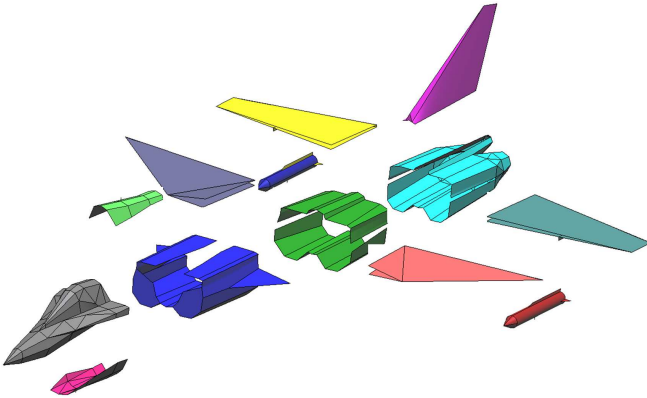


Fig. 18. Decomposition of the morphed Rafale; note that no artificial internal surfaces are used

is obtained for the simulation case both for the decomposed case (using the proposed method) and for the single domain case (using only RWGs in the discretization); the fast solver used is an ACA with the same compression tolerance of 1×10^{-3} for both the (reference) single-domain and the DD case. The ILU is used as preconditioner for the single domain reference and the inner sub-domains of the decomposed case; note that in the decomposed case the ILU parameters such as

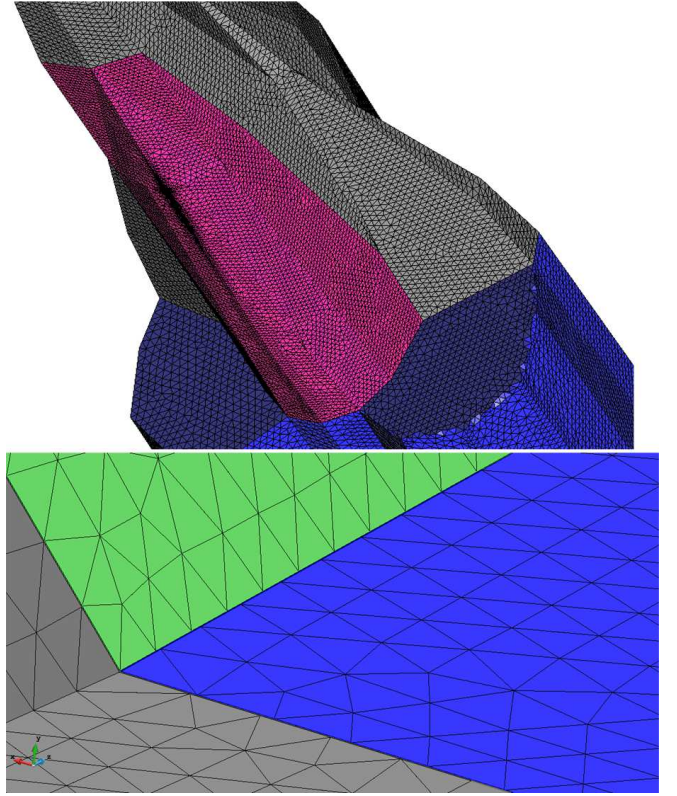


Fig. 19. Non-conformal nature of the mesh

fill-in and *droptol* (see [8] for details), are set *independently* for each sub-domain, giving great versatility for multi-scale structures. For multi-scale structures, the *droptol* depends on the smaller elements of the matrix; while the *fill-in* depends on the different scales in the problem (e.g. the larger the differences, the larger the *fill-in* needed to obtain a stable decomposition). It is remarked again that the use of the inner preconditioner for the DD proposed is up to the users need, and the ILU is used here for illustrative purposes and widespread use in electromagnetics. The single domain mesh contains 294 645 RWGs, and the same CFIE-EFIE formulation for the closed-open parts have been used. The computational statistics of the test cases are presented in table II.

The statistics presented in table II can be summarized as follows; for the single domain case the “*fill-in*” parameter was set to 1, 2 and 3, obtaining in all cases unstable results, where the stability is measure using the *Condest* [10], [11]; for the unstable cases the *Condest* is higher than $1e+10$; for the single domain - ILU scheme, the “*fill-in*” of 4 results in a stable decomposition; for the DD case most of the *Condest* estimated are lower than 1000 (except for the domains where the blade antennas are included, where the *Condest* do not go over $1e+9$); the *Condest* are not reported for the sake of space and clarity. In the DD case (“*This work*”) each domain is treated independently, so the “*fill-in*” parameter is set individually for each domain, according to the requirements; the numbers are presented in the same order as the domains (domain 1 being the tip of the aircraft, domain 3, 11, 12 and 13 where the blade antennas are located). The “peak memory” column states

TABLE II
COMPUTATIONAL STATISTICS COMPARISON BETWEEN SINGLE AND DECOMPOSED DOMAIN PEC RAFALE

Solver	ILU <i>fill-in</i>	Iterations	Peak memory (GB)	Precond. time (h:m:s)	Sol. time (h:m:s)
<i>Single Dom. ILU</i>	4	39	31.5	4:08:57	0:11:19
<i>This work</i>	1/1/2/1...2/2/2	19	5.7	0:32:51	0:06:32
<i>Single Dom. MR-ILU</i>	4*	463	2.7	0:15:00	1:24:0

the memory needed for the preconditioner; in the DD case it takes into account the ILU memory plus the inner solver compressed matrix. “*Precond. time*” stands for the time spent building the preconditioner (in the DD case the ILU’s are built in parallel); “*Solv. time*” stands for the iterative solution of the linear system.

We remark here that obviously the number of iterations is only a very partial indicator of efficiency: the cost of the preconditioner has of course to be factored in as well. In the given example, the ILU provides a fast convergence but at the cost of significant memory requirement, and the preconditioning overhead largely overcomes the solution time. The use of ILU on the sub-domains intrinsically requires a much smaller time overhead and memory occupation; this is also due to the flexibility in tailoring the (ILU) preconditioning parameters to the need of each sub-domain. In this sense, the comparison with the ILU on the single-domain may appear a debatable benchmark, since the latter is known to have poor performance on multi-scale problems. Therefore, we have also benchmarked our DD results with the hybrid MR-ILU approach proposed in [11] and successfully used to solve multi-scale structures (the hybrid MR-ILU has been applied the single domain reference). In the MR-ILU scheme, the ILU preconditions only a portion of the overall matrix, the rest being preconditioned by the MR (see [11] for details); therefore, to avoid confusion, the ILU parameter is flagged by a “*”. The MR-ILU hybrid results the most memory- and generation time efficient; the proposed DD scheme however provides an even better overall convergence speed, which therefore appears very remarkable.

The presented statistics show the capability of the proposed approach to deal with multi-scale ill conditioning, while preserving great versatility in terms of sub-domains treatment (independent meshing, individually precondition each problem, use of a desired fast solver, etc.). The obtained results (equivalent current density) for the test cases are shown in figure 20 where the imaginary part of the equivalent current density in dB/m is compared; figure 21 shows equivalent current density (real part in dB/m) on one rocket; in the DD case it can be note the non-conformity between the rocket body and the rocket bay under the wing. Figures 22 and 23 presents the equivalent current density in A/m for single and DD analysis respectively, with a detail of the current distribution in the $\lambda/4$ monopole. As expected from the test case, the higher coupling to the structure is on the $\lambda/4$ monopole antennas (only the on in the back of the cockpit shown for the sake of space).

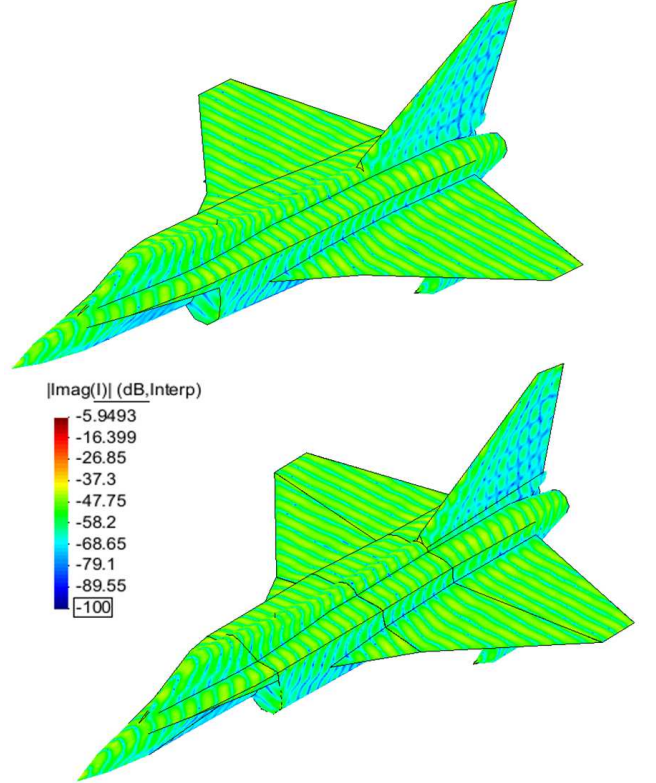


Fig. 20. Imaginary part of the current density in dB/m; single (up) and decomposed (down)

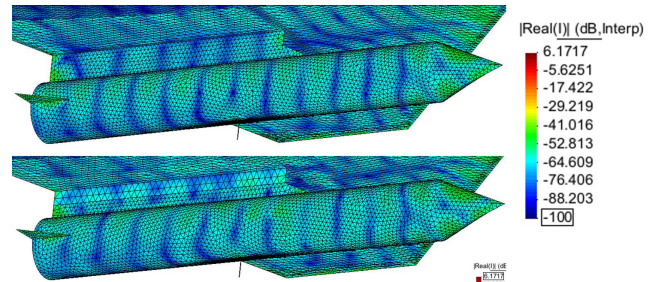


Fig. 21. Real part of the current density in dB/m; single (up) and decomposed (down)

F. Complex Test Case at Higher Frequency

Once the effectiveness of the proposed DD has been demonstrated in section IV-E, the same morphed version of the Rafale aircraft is simulated at the higher frequency of 1.2 GHz; the whole structure is discretized at $\lambda/10$ except the large planar surfaces (wings and tail-wing) discretized at $\lambda/8$. A port excitation is used in this case to excite one of the $\lambda/4$ monopoles (which have the same discretization size as before, but have been scaled accordingly to keep the same

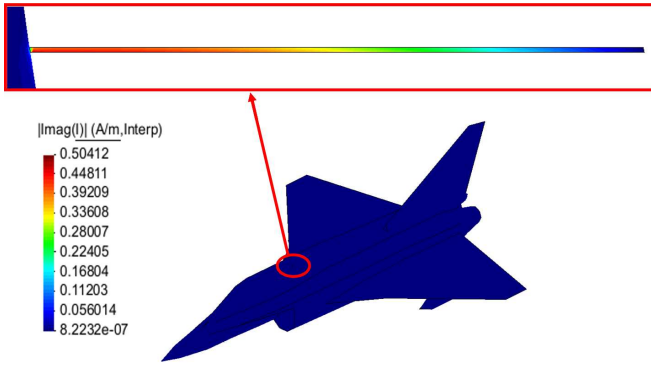


Fig. 22. Imaginary part of the current density in A/m for the single domain case (ACA+ILU); a zoom in is made on the antenna in order to confirm the higher coupling of the impinging wave

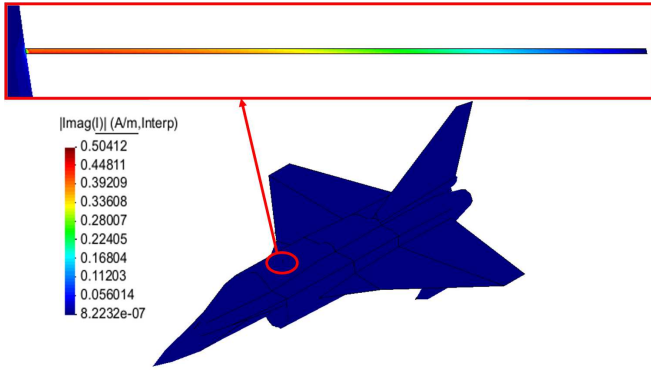


Fig. 23. Imaginary part of the current density in A/m for the decomposed domains case (This work scheme); a zoom in is made on the antenna in order to confirm the higher coupling of the impinging wave

$\lambda/4$ length). The structure is 56λ from tip to tail, the same decomposition was maintained as in the previous example; the test case has now 742 157 RWGs + 6 822 h-RWGs for a total of 748 979 unknowns. The discretization for this test case is mostly conformal due to the small wavelength. The current distribution (imaginary part dB/m) is shown in figure 24.

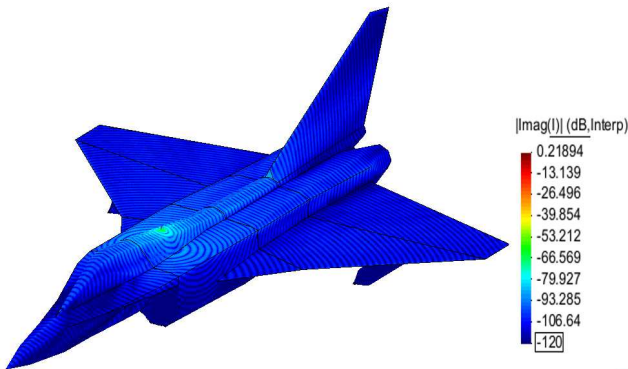


Fig. 24. Imaginary part of the current density distribution for a feed blade antenna @ 1.2 GHz

For this test case, the inner preconditioner parameters were kept unchanged respect to the section IV-E; the preconditioner generation time is 5 minutes for this case, as the near field matrices used to generate the ILU are sparser (the near field

is halved respect to the 600 MHz case, even if the number of unknowns are roughly the double). The $1e-6$ residual is reached in 10 iterations and the solution time is 10 minutes. Interesting facts are to be remarked here; the number of iterations is lowered respect to the case in section IV-E for various reasons, one is the fact that due to the small wavelength, the discretization is quite homogeneous in the whole structure; the second reason are the evanescent modes decay, whose effects were studied in sections IV-C and IV-B. The final reason is that with the port excitation, the DD matches the solutions of the different sub-domains using the natural propagation of the different modes (waves start propagating from the excited sub-domains and are coupled to the rest of the sub-domains through the outer iterations), while in the plane wave, every sub-domain has a given excitation which is independent from each other and must be matched.

G. Hybrid Open/Closed Multi-scale Test Case

In this section the capabilities to perform the decomposition on hybrid closed/open structures are demonstrated; a simplified version of the aircraft in the previous section is used (with the same impinging 600 MHz plane wave). The aircraft wings have been intentionally shrunk to single open surfaces, where the EFIE use is mandatory; the decomposition cuts the wings as shown in figure 25. The discretization in this test case combines conformal and non-conformal characteristics.

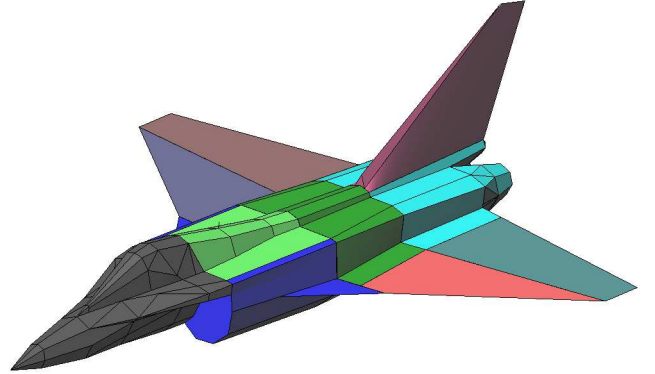


Fig. 25. Decomposition of the hybrid open/closed morphed Rafale

The imaginary and real parts of the current density are shown in figures 26 and 27 respectively.

The agreement with respect to the entirely closed test case is quite good (letting apart the fact that the wings are now open surfaces and the rockets are no longer present); this test case uses 200 800 RWG + 2380 h-RWG, which signifies a reduction of 1/4 of the number of unknowns with respect to the completely closed case; this test case takes 20 iterations to converge to the same residual (1×10^{-6}), as the EFIE operator is not as well conditioned as the CFIE.

V. CONCLUSIONS

We have presented a Domain-Decomposition (DD), Tear-and-Interconnect approach for the EFIE and CFIE, for open, closed, and open-closed structures. It employs transmission

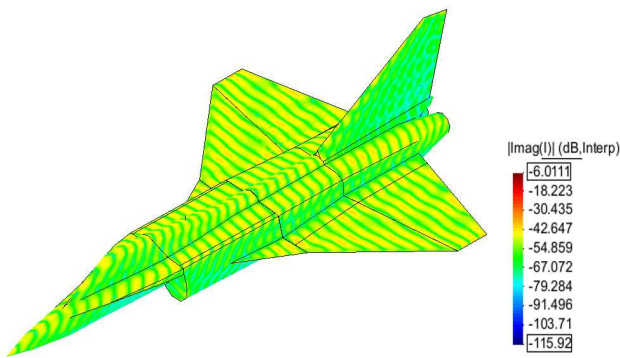


Fig. 26. Imaginary part of the current density (dBA/m) for the hybrid open/closed morphed Rafale

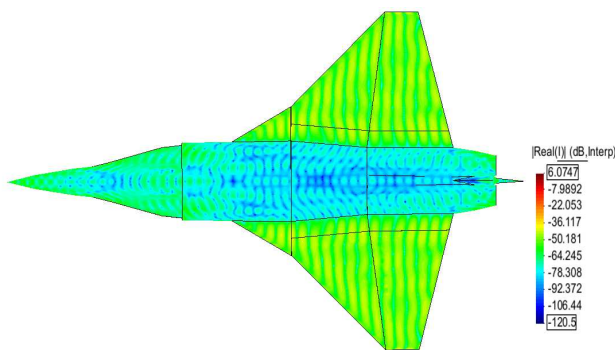


Fig. 27. Real part of the current density (dBA/m) for the hybrid open/closed morphed Rafale

conditions exploiting a Discontinuous Galerkin scheme, which allows non-conformal meshes in adjacent domains. The DD allows flexible inner-outer iteration loops that provide fast convergence and are applicable to any fast factorization. Domain augmentation is proposed to expedite convergence, and effected employing only a portion of the near-field interactions matrix. Numerical examples have demonstrated the effectiveness of the proposed approach. The presented approach is self-contained and easy to apply to existing fast codes.

Several upgrades can be made to the proposed scheme, as for example: testing different inner-outer Krylov subspace solvers combinations; use of direct solvers for the inner subdomains solutions, in order to accelerate the solving phase; and the inclusion of the MR-ILU preconditioning in the inner solvers.

ACKNOWLEDGMENT

REFERENCES

- [1] A. W. Glisson and D. R. Wilton, "Simple and efficient numerical methods for problems of electromagnetic radiation and scattering from surfaces," *IEEE Trans. Antennas Propag.*, vol. AP-28, pp. 593–603, Oct. 1980.
- [2] W. C. Chew, J. M. Jin, E. Michielssen, and J. M. Song, *Fast and efficient algorithms in computational electromagnetics*. Boston, MA: Artech House, 2001.
- [3] J. M. Song and W. C. Chew, "Multilevel fast multipole algorithm for solving combined field integral equation of electromagnetic scattering," *Microwave and Optical Technology Letters*, vol. 10, pp. 14–19, Sept. 1995.
- [4] S. Seo and J. Lee, "A fast IE-FFT algorithm for solving PEC scattering problems," *IEEE Trans. Magn.*, vol. 41, pp. 1476–1479, May 2005.
- [5] E. Michielssen and A. Boag, "A multilevel matrix decomposition algorithm for analyzing scattering from large structures," *IEEE Transactions on Antennas and Propagation*, vol. 44, pp. 1086–1093, Aug. 1996.
- [6] K. Zhao, M. N. Vouvakis, and J. F. Lee, "The adaptive cross approximation algorithm for accelerated method of moments of EMC problems," *IEEE Trans. Electromagn. Compat.*, vol. 47, pp. 763–773, Nov. 2005.
- [7] J. M. Tamayo, A. Heldring, and J. M. Rius, "Multilevel adaptive cross approximation," *IEEE Trans. Antennas Propag.*, vol. 59, pp. 4600–4608, Dec 2011.
- [8] Y. Saad, "ILUT: a dual threshold incomplete ilu factorization," Tech. Rep. UMSI-92-38, Minnesota Supercomputer Institute, University of Minnesota, Minneapolis (MN, USA), 1992.
- [9] J. Lee, J. Zhang, and C. Lu, "Incomplete lu preconditioning for large scale dense complex linear systems from electromagnetic wave scattering problems," Tech. Rep. 342-02, Department of Computer Science, University of Kentucky, Lexington (KY, USA), 2002.
- [10] T. Malas and L. Gurel, "Incomplete LU preconditioning with the multilevel fast multipole algorithm for electromagnetic scattering," *SIAM J. Sci. Comput.*, vol. 29, pp. 1476–1494, June 2007.
- [11] F. Vipiana, M. A. Francavilla, and G. Vecchi, "EFIE modeling of high-definition multi-scale structures," *IEEE Trans. Antennas Propag.*, vol. 58, pp. 2362–2374, July 2010.
- [12] F. Vipiana, P. Pirinoli, and G. Vecchi, "A multiresolution method of moments for triangular meshes," *IEEE Trans. Antennas Propag.*, vol. 53, pp. 2247–2258, July 2005.
- [13] F. P. Andriulli, F. Vipiana, and G. Vecchi, "Hierarchical bases for non-hierarchical 3D triangular meshes," *IEEE Trans. Antennas Propag.*, vol. 56, pp. 2288–2297, Aug. 2008.
- [14] F. Vipiana, P. Pirinoli, and G. Vecchi, "Spectral properties of the EFIE-MoM matrix for dense meshes with different types of bases," *IEEE Trans. Antennas Propag.*, vol. 55, pp. 3229–3238, Nov. 2007.
- [15] E. Suter and J. R. Mosig, "A subdomain multilevel approach for the efficient MoM analysis of large planar antennas," *Microwave and Optical Technology Letters*, vol. 26, pp. 270–277, Aug. 2000.
- [16] V. V. S. Prakash and R. Mittra, "Characteristic basis function method: a new technique for efficient solution of method of moments matrix equation," *Microwave Opt. Technol. Lett.*, vol. 36, p. 95100, Jan. 2003.
- [17] L. Matekovits, G. Vecchi, G. Dassano, and M. Orefice, "Synthetic function analysis of large printed structures: the solution sampling approach," in *Proc. of IEEE Int. Symp. Antennas Propag.*, (Boston MA, USA), Jun. 2001.
- [18] L. Matekovits, V. A. Laza, and G. Vecchi, "Analysis of large complex structures with the synthetic-functions approach," *IEEE Trans. Antennas Propag.*, vol. 55, pp. 2509–2521, Sept. 2007.
- [19] N. Ozdemir, D. Gonzalez-Ovejero, and C. Craeye, "On the relationship between multiple-scattering macro basis functions and Krylov subspace iterative methods," *IEEE Trans. Antennas Propag.*, vol. 61, pp. 2088–2098, April 2013.
- [20] C. Brennan, P. Cullen, and M. Condon, "A novel iterative solution of the three dimensional electric field integral equation," *IEEE Trans. Antennas Propag.*, vol. 52, pp. 2781–2784, Oct. 2004.
- [21] W. D. Li, W. Hong, and H. X. Zhou, "An IE-ODDM-MLFMA scheme with DILU preconditioner for analysis of electromagnetic scattering from large complex objects," *IEEE Trans. Antennas Propag.*, vol. 56, pp. 1368–1380, May 2008.
- [22] Z. Peng, X. C. Wang, and J. F. Lee, "Integral equation based domain decomposition method for solving electromagnetic wave scattering from non-penetrable objects," *IEEE Trans. Antennas Propag.*, vol. 59, pp. 3328–3338, Sept. 2011.
- [23] Z. Peng, K. Lim, and J. F. Lee, "Non-conformal domain decomposition methods for solving large multiscale electromagnetic scattering problems," *Proceedings of the IEEE*, vol. 101, no. 2, pp. 298–319, 2012.
- [24] S. C. Lee, M. Vouvakis, and J. F. Lee, "A non-overlapping domain decomposition method with non-matching grids for modeling large finite antenna arrays," *J. Comput. Phys.*, vol. 203, pp. 1–21, 2005.
- [25] O. Wiedenmann and T. F. Eibert, "A domain decomposition method for boundary integral equations using transmission condition based on the near-zone couplings," *IEEE Trans. Antennas Propag.*, vol. 62, pp. 4105–4114, Aug. 2014.
- [26] D. Pissort, E. Michielssen, D. V. Ginste, and F. Olyslager, "A rank-revealing preconditioner for the fast integral equation based characterization of electromagnetic crystal devices," *Microwave and Optical Technology Letters*, vol. 48, pp. 783 – 789, 2006.

- [27] X. Wang, Z. Peng, and J. F. Lee, "A new integral equation based domain decomposition method for electromagnetic analysis of large multi-scale problems," in *Proc. of IEEE Int. Symp. Antennas Propag.*, 2012.
- [28] Z. Chen, Q. Du, and J. Zou, "Finite element methods with matching and nonmatching meshes for maxwell equations with discontinuous coefficients," *SIAM J. Num. Anal.*, vol. 37, pp. 1542–1570, 2000.
- [29] S. M. Rao, D. R. Wilton, and A. W. Glisson, "Electromagnetic scattering by surfaces of arbitrary shape," *IEEE Trans. Antennas Propag.*, vol. 30, pp. 409–418, May 1982.
- [30] Y. Saad and M. Schultz, "GMRES: A Generalized Minimal Residual Algorithm for Solving Nonsymmetric Linear Systems," *SIAM J. Sci. Stat. Comput.*, no. 7, pp. 856–869, 1986.
- [31] Z. Peng, K. H. Lim, and J. F. Lee, "A discontinuous Galerkin surface integral equation method for electromagnetic wave scattering from non-penetrable targets," *IEEE Trans. Antennas Propag.*, vol. 61, pp. 3617–3628, July 2013.
- [32] X. Wang, *A Domain Decomposition Method for Analysis of Three-dimensional Large-scale Electromagnetic Compatibility Problems*. PhD Thesis, The Ohio State University, 2012.
- [33] Z. Peng, V. Rawat, and J. F. Lee, "One way domain decomposition method with second order transmission conditions for solving electromagnetic wave problems," *J. Comput. Phys.*, vol. 229, pp. 1181–1197, 2010.